



HAL
open science

On the low temperature limits for cryogenic etching: A quasi in situ XPS study

Felipe Cemin, Aurélie Girard, Christophe Cardinaud

► To cite this version:

Felipe Cemin, Aurélie Girard, Christophe Cardinaud. On the low temperature limits for cryogenic etching: A quasi in situ XPS study. *Applied Surface Science*, 2023, 637, pp.157941. 10.1016/j.apsusc.2023.157941 . hal-04186858

HAL Id: hal-04186858

<https://hal.science/hal-04186858>

Submitted on 24 Aug 2023

HAL is a multi-disciplinary open access archive for the deposit and dissemination of scientific research documents, whether they are published or not. The documents may come from teaching and research institutions in France or abroad, or from public or private research centers.

L'archive ouverte pluridisciplinaire **HAL**, est destinée au dépôt et à la diffusion de documents scientifiques de niveau recherche, publiés ou non, émanant des établissements d'enseignement et de recherche français ou étrangers, des laboratoires publics ou privés.

On the low temperature limits for cryogenic etching: a *quasi in situ* XPS study

Felipe Cemin ^{a,*}, Aurélie Girard ^{a,*}, Christophe Cardinaud ^a

^a Nantes Université, CNRS, Institut des Matériaux de Nantes Jean Rouxel (IMN), 44300
Nantes, France

* +33 240376310, felipe.cemin@cnrs-imn.fr, aurelie.girard@cnrs-imn.fr

Abstract:

The cryogenic plasma etching of silicon for nano- and microelectromechanical devices is known to show an optimal operating temperature around -100 °C. The physicochemical mechanisms occurring beyond this limit, however, are not often discussed. Thus, to explore the adsorption of residual gases on the uppermost surface of a Si/SiO₂ wafer at $-100 \leq T \leq -147$ °C, we performed a comprehensive, *quasi in situ* X-ray photoelectron spectroscopy (XPS) study. Precisely, the cooling down of the sample was performed in a typical plasma-etching reactor at a residual pressure of 10^{-4} Pa, being afterwards transferred to the XPS chamber at a constant temperature under high vacuum. We report that water build-up on the surface becomes a major issue for $T < -120$ °C, as detected in the O 1s spectra and modelled by QUASES-Generate. The thickness of the H₂O layer increases exponentially as the surface temperature decreases, following an anti-Arrhenius behavior. At -147 °C, the overlayer thickness is estimated to ~ 125 Å, thus, the silicon is barely probed by XPS. Adsorbed fluorine can also be detected at low temperatures, although less markedly. Finally, the effect of the temperature-dependent Fermi level change on the Si 2p peak binding energy is discussed.

Keywords: X-ray photoelectron spectroscopy, cryogenic plasma etching, semiconductors, water adsorption, physisorption energy, residual gases.

1 Introduction

The advent of silicon etching at cryogenic temperatures has allowed obtaining microelectromechanical systems (MEMS) and through-silicon via (TSV) with high aspect ratio, controllable sidewall profiles, and high selectivity [1–4]. Behind these technological advances lie several physicochemical mechanisms and phenomena occurring on the uppermost atomic layers of the cooled Si surface. Among them, the formation of a siliconoxyfluoride (SiO_xF_y) passivation layer under SF_6 (or SiF_4) / O_2 plasmas is nowadays accepted as one of the key steps of the cryogenic process [4–6]. Indeed, this layer preserves the Si sidewalls from ion bombardment, whilst is easily etched at the trench bottom, due to the unidirectional flux of the ions, *i.e.*, anisotropy is achieved.

There is a consensus on the temperature to grow an optimal SiO_xF_y layer, typically around $-100\text{ }^\circ\text{C}$ [4], even if the process is very sensitive to small variations in temperature [7]. Moreover, defects such as bowing, undercutting, and crystallographic faceting are minimized when the Si temperature is at about $-100\text{ }^\circ\text{C}$ [8,9]. Regarding the operating limits, previous studies showed that temperatures higher than $-80\text{ }^\circ\text{C}$ yield isotropic Si etching [5] due to the SiO_xF_y layer thickness decrease or partial desorption [6,10]. On the other hand, the use of too low temperatures (below $-130\text{ }^\circ\text{C}$) resulted in an “etch stop” phenomenon [11], due to strong condensation of SF_6 on the Si surface [12–14]. Although these investigations highlight an operating temperature window in the cryogenic process, they do not focus on the singularities and atomic-scale mechanisms at the temperature limits, particularly for $T < -120\text{ }^\circ\text{C}$.

The effect of decreasing the temperature of a solid surface exposed to a gas/plasma phase is to modify the surface kinetics of the adsorbed atoms and molecules, as well as to limit or even suppress thermally activated chemical reactions. For instance, it is generally noticed an increase in the amount and variety of physisorbed species, longer residence times, and reduced surface diffusion at low temperatures. Importantly, the adsorbed species stem from

both the working gases of the etching process and the residual gases present in the reactors. The latter are due to leaking, outgassing, and sputtering from the chamber walls and might significantly affect the physicochemical mechanisms on the cooled surface if the temperature is sufficiently low. In this regard, Bartha *et al.* [15] were the first to explain the mechanisms of the Si cryogenic etching under SF₆ plasma [12] taking into account the presence of oxygen as a contaminant, *i.e.*, not intentionally added as a working gas. Nevertheless, reports on the interaction of residual gases with cooled surfaces are rare or limited.

Here, a comprehensive X-ray photoelectron spectroscopy (XPS) study has been performed on the surface of a Si wafer at different cryogenic temperatures ($-100 \leq T \leq -147$ °C) under high vacuum level. The aim was to investigate specifically the adsorption mechanisms of residual gases and contaminants found in a typical plasma-etching reactor, as a previous step before the surface processing. This allowed us to identify and understand the major physicochemical modifications taking place on the studied surface, as well as to establish a low temperature limit for Si cryogenic etching as a function of residual water adsorption. The general trends could be generalized to other materials in semiconductors technology.

2 Materials and methods

X-ray photoelectron spectroscopy was used to study the chemical state and composition of the surface of a crystalline, p-type boron doped Si(100) wafer, resistivity of 10–20 Ω cm, and dopant concentration $\sim 8.8 \times 10^{14}$ at. cm⁻³. The 500 μm thick, 10 × 10 mm² Si sample is covered with a native oxide (SiO₂) layer, *i.e.*, no pretreatment processes such as chemical or plasma cleaning were used. The experiments were performed in the Optimist facility [16,17], see Fig. S1 (Supplementary Material), composed of two vacuum chambers: a homemade inductively coupled plasma (ICP) reactor and an XPS analysis chamber. The former is typically used in plasma etching processing under SF₆, SiF₄, and C₄F₈ reactive gases, alone or

in mixture with Ar, N₂, and O₂, and its base pressure is $\sim 4 \times 10^{-4}$ Pa. The latter is only dedicated to XPS analysis and has a base pressure of around 5.0×10^{-7} Pa. The chambers are connected by an intermediate tube where differential pumping is executed. The sample is placed on a holder within a moving rod, and the temperature of the holder is regulated by a liquid nitrogen circulation and an imbedded thermal resistance. The temperature is controlled by a PID device (range of variation ± 0.1 °C). The moving rod was specifically designed and made for the Optimist facility. The sample holder can be moved from the ICP reactor to the XPS chamber (and *vice versa*) by simple translation of the rod, while maintaining the sample temperature constant and keeping it under high vacuum. Therefore, the sample is conserved on the same temperature-stabilized holder during the entire process and the analysis is performed in a *quasi in situ* condition. This is very helpful, since most of the species involved in the process desorb if the sample is brought to the room temperature (RT) prior to analysis.

The cooling down experiments reported in this article were carried out in the ICP reactor under vacuum, without any gas or plasma exposure, to evince exclusively the adsorption at low temperatures of residual gases or contaminants present in the processing reactor. A single Si substrate was cooled down from RT (+25 °C) to -100 , -120 , -135 , -141 , and -147 °C, and lastly heated up to +25 °C. After each substrate temperature change and stabilization (for 7 min) in the reactor, the sample holder was moved from the ICP chamber to the analysis chamber for XPS measurement. We notice that additional experiments were conducted to verify the effect of the low temperature on the adsorption of residual gases or contaminants exclusively in the XPS chamber, *i.e.*, the Si wafer was cooled down directly in the analysis chamber. The results are shown in the Supplementary Material (Fig. S2 and Table S1) and demonstrate that the contamination of the Si surface is insignificant into the XPS chamber at temperatures as low as -164 °C, due to the much lower base pressure level.

XPS analysis were performed with an Al K α monochromatized X-ray source (SPECS XR 50 M and Focus 500) operated at 400 W. The analyzer (SPECS Phoibos 150HR) runs in a fixed transmission and a medium area mode. Survey scans were acquired at 30 eV pass energy (PE) with 0.5 eV steps and narrow scans at PE = 14 eV with 0.05 eV steps. The experimental overall resolution was estimated from the full width at half maximum (FWHM) of the Ag 3d_{5/2} peak at PE = 14 eV, which was 0.55 eV at RT. The CasaXPS processing software [18] was used to perform peak fitting and to estimate the relative atomic concentrations. All narrow XPS spectra were energy-corrected by the adventitious C 1s spectral component (at 285.0 eV [19]), as shown in Fig. S3 (Supplementary Material). A U 2 Tougaard background was applied for the core levels, to subtract the contribution of inelastically scattered photoemitted electrons. The peak fitting was performed using a simple Gaussian-Lorentzian (70%-30%) product line shape for all elements, and the FWHM values for a same peak varied slightly between the different samples. In addition, the intensity I of the photoelectrons emitted after attenuation due to an overlayer of thickness d was calculated by the Beer-Lambert law, $I = I_0 \exp(-d/\lambda)$, where I_0 is the intensity of photoelectrons emitted by a clean surface and λ is the attenuation length. The latter is also called inelastic electron mean free path (IMFP) and was calculated from the TPP-2M formula [20] using the QUASES-Tougaard software. Finally, the thickness of the overlayer was estimated through the modelling of the inelastic scattering background using the QUASES-Generate software [21]. The scale factor was close to 1 (from 0.95 to 0.99) in all cases.

3 Results and Discussion

Fig. 1a shows the XPS survey spectra of the Si wafer surface at three selected temperatures: +25 °C (RT), -100 °C (typical temperature used in Si cryogenic etching), and -147 °C (the lowest temperature probed in this study). The cooling down of the surface was performed in the ICP reactor, under high vacuum, and the sample was transferred to the XPS

chamber at the same temperature for *quasi in situ* analysis. At RT, three main peaks related to the Si 2p, O 1s, and C 1s photoelectrons are observed, along with the Si 2s, O 2s and O_{KLL} secondary contributions. The source of oxygen is mainly due to the native oxide layer on the Si wafer surface, while carbon is present as a surface contaminant. A very similar XPS spectrum is obtained for the Si wafer surface at $-100\text{ }^{\circ}\text{C}$, except for the presence of a small F 1s peak. The surface contamination by residual fluorine at low temperatures will be discussed in Section 3.3. At $-147\text{ }^{\circ}\text{C}$, however, a strong increase in intensity of the O 1s peak is noticed, whereas the Si 2p (and Si 2s), C 1s, and F 1s peaks nearly disappeared.

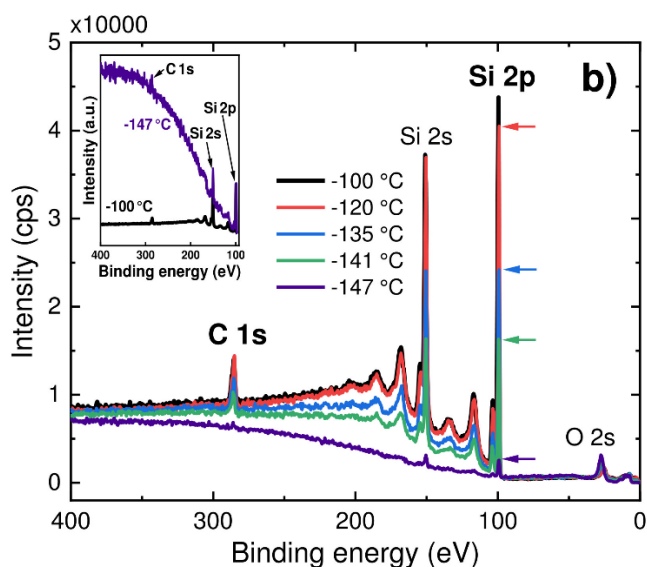
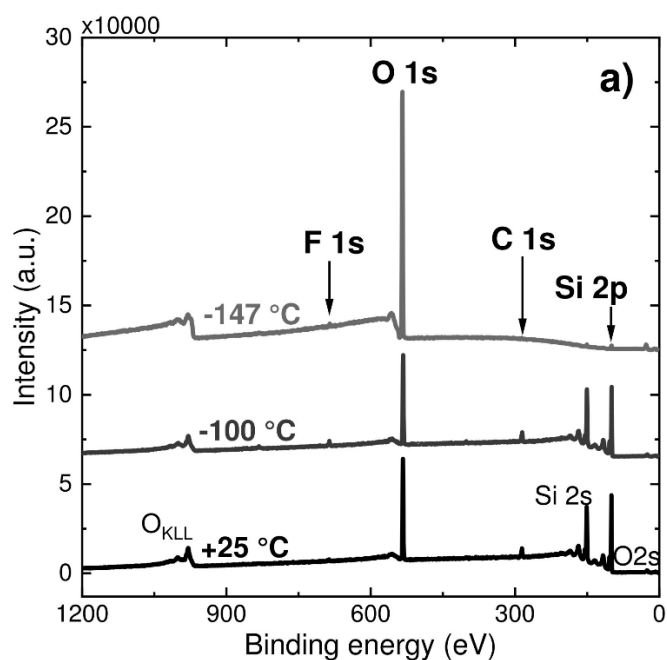


Fig. 1. a) Wide scan spectra of the surface analyzed by XPS, at three selected temperatures of the Si wafer under high vacuum and b) evolution of the 400 to 5 eV binding energy region as a function of the Si temperature. The arrows alongside the Si 2p peak indicate the intensity maxima for the different temperature conditions. The inset shows the -100 and -147 °C spectra normalized to the intensity of the respective Si 2p peaks.

To understand this pronounced change, a series of temperatures between -100 and -147 °C were investigated. Fig. 1b shows the evolution of the XPS spectra in the $400 \rightarrow 5$ eV binding energy (BE) range as a function of the Si wafer temperature. A clear modification in both the peak intensity signal and the background level is noticed from $T = -135$ °C. First, the C 1s, Si 2s and Si 2p peaks are reduced in intensity as the temperature becomes lower, indicating that a fraction of these photoelectrons is lost due to inelastic scattering before reaching the material surface. Second, the background shape in the 400 to 100 eV range changes, which could be related to a variation in the depth distribution of carbon and silicon elements in the analysis volume at lower temperatures. Indeed, photoelectrons that are emitted deeper in the solid are more likely to lose their energy in inelastic collisions and, therefore, contribute further to the background signal [22,23]. This is clearly the case for the -147 °C sample, see Fig. 1b (inset), where the background intensity at high binding energies is much higher compared to that of the elastically scattered Si 2p photoelectrons (the intensities were normalized to the respective Si 2p peaks).

The findings mentioned above suggest that an overlayer is formed on the top of the Si wafer at temperatures lower than -120 °C. The composition of this layer shows a great content of oxygen element, as demonstrated in Fig. 1a for the -147 °C sample. In the next section, the O 1s XPS spectra will be detailed along with the relative atomic contents, and a physisorption mechanism will be proposed.

3.1 Water physisorption on Si/SiO₂ at low temperatures

The O 1s XPS narrow scans of the studied surfaces are plotted in Fig. 2a as a function of the Si wafer temperature. The main peak observed for the +25 °C sample is progressively shifted to higher binding energies as the substrate temperature becomes lower, with an increment of +1.25 eV at –147 °C compared to the RT sample. This is due to the different oxygen-containing chemical species present on the analyzed surface, which are identified in the suggested peak fitting in Fig. 2b-e.

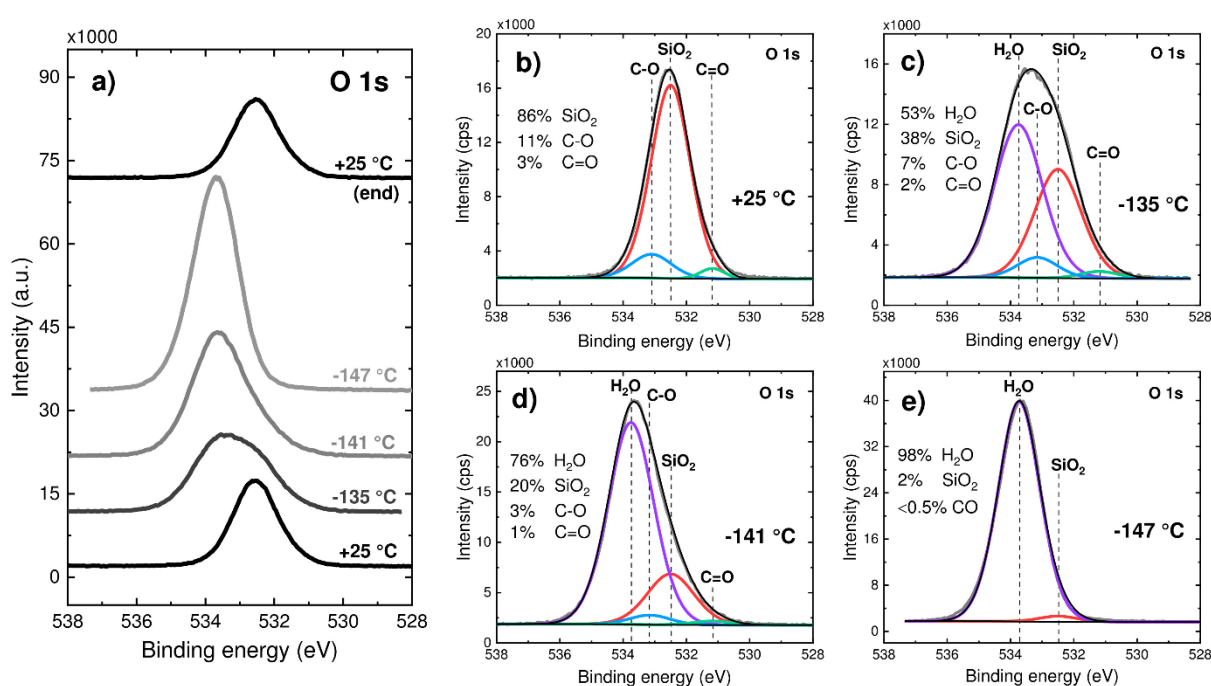


Fig. 2. a) Evolution of the O 1s XPS peak shape as a function of the Si wafer temperature, under vacuum, and b-e) the components proposed for each O 1s XPS spectrum shown in (a) along with the estimated amount of the chemical bonding/species identified in the same spectra.

At RT (Fig. 2b), the main peak centered at 532.5 eV corresponds to the SiO₂ native oxide present on the wafer surface, in addition to the carbon-related compounds identified at 531.2 eV (C=O) and 533.15 eV (C–O) [24]. The presence of organic groups as contaminants is well known in surface analysis [25], being also verified in the respective C 1s spectra, see Fig. S3 (Supplementary Material). A very similar O 1s XPS spectrum is obtained at –100 °C (not

shown). When the Si wafer is cooled down to $-135\text{ }^{\circ}\text{C}$ (Fig. 2c), however, a new peak is observed at 533.75 eV , which is associated with adsorbed water on inorganic surfaces [26–29]. The H_2O peak corresponds to approximately 53% of the O 1s photoelectrons emitted at $-135\text{ }^{\circ}\text{C}$, 76% at $-141\text{ }^{\circ}\text{C}$ (Fig. 2d), and 98% at $-147\text{ }^{\circ}\text{C}$ (Fig. 2e), according to our peak fitting. Concomitantly, the fraction of oxygen atoms stemming from the native SiO_2 layer decrease to approximately 2% at $-147\text{ }^{\circ}\text{C}$, suggesting that the Si substrate is masked by a relatively thick ($> 10\text{ nm}$) overlayer of adsorbed water. It is interesting to note that, after heating up the same Si wafer to $+25\text{ }^{\circ}\text{C}$, the O 1s peak recovers its intensity and initial BE of 532.5 eV (Fig. 2a, $+25\text{ }^{\circ}\text{C}$ “end” spectrum), *i.e.*, water disappears. We highlight that X-ray beam damage on the water layer is not considered in this study, since the O 1s peak shape and position for a given temperature do not change notably over total acquisition time ($\sim 115\text{ min}$).

Temperature ($^{\circ}\text{C}$)	O 1s (at. %)	Si 2p (at. %)	C 1s (at. %)	F 1s (at. %)
+25	27	63	9	<1
-100	27	60	11	2
-120	28	57	12	3
-135	42	48	8	2
-141	58	33	7	2
-147	93	4	2	1
+25 (end)	25	63	10	2

Table 1. Relative atomic concentrations (at.%) of the analyzed surface at different Si wafer temperatures, under vacuum, from the XPS narrow scans.

Besides the different chemical species, Fig. 2 also reveals that the intensity of the O 1s spectra changes with temperature, with a maximum intensity at the lowest temperature. The relative atomic concentrations estimated from narrow XPS scans are presented in Table 1. One notices that from RT to $-120\text{ }^{\circ}\text{C}$, the amount of oxygen remains constant at $\sim 27\%$ on the analyzed surface. Then, the oxygen atomic concentration rises to 42% at $-135\text{ }^{\circ}\text{C}$ and reaches 93% at $-147\text{ }^{\circ}\text{C}$. As indicated in Fig. 2, the huge increase in the O 1s signal at low temperatures is likely due to water build-up on the Si surface, from the vapor phase.

Adsorption of residual water at $-150\text{ }^{\circ}\text{C}$ on the top of a SF_x adsorbed layer on Si was also detected by *quasi in situ* XPS previously [13]. The water molecules mainly stem from outgassing of the reactor walls and metallic parts, which are known to be covered with several layers of H_2O [30]. Moreover, real or virtual leaks are a continuous source of water vapor and other residual gases, such as H_2 , O_2 , N_2 , CO_2 , and Ar, in vacuum systems. Under equilibrium conditions, the water molecules travelling inside the reactor may be either dragged in the pumping system and evacuated, or impinge on a surface, lose their kinetic energy, and eventually adsorb on it. In the latter case, molecules that collide with a cooled surface might condense, be retained by physical adsorption, or at least have their residence times increased. Accordingly, our results indicate that water adsorption is enhanced at lower temperatures, *i.e.*, the cooled Si substrate act as a “cryogenic pump” for residual water molecules.

In order to further investigate the water adsorption mechanisms, the intensity of the H_2O component in each O 1s XPS peak was considered. Note that the intensity in XPS studies is usually substituted for the area under the spectrum, which is proportional to the amount of a chemical specie or environment. Fig. 3a shows that the area of the peak ascribed to oxygen in the H_2O molecule increases exponentially as temperature decreases from -100 to $-147\text{ }^{\circ}\text{C}$. The experimental points were fitted to an exponential decay function, and the obtained R^2 was equal to 0.9956. This water adsorption dependence on temperature suggests an inverse (or anti-)Arrhenius behavior [31], since adsorption gets faster as temperature decreases. In other words, the amount of water follows an $\exp(E/kT)$ law, where E is the characteristic energy of the adsorption/desorption process, T is the surface temperature in Kelvin, and k is the Boltzmann constant. The Arrhenius plot is presented in Fig. 3b, where the area of the H_2O peak in XPS is plotted logarithmically versus $1/T$ (K). The resulting positively sloped line ($R^2 = 0.9979$) yields $E = 0.169\text{ eV}$ (± 0.006). We highlight that this estimation gives primarily

the magnitude of the adsorption/desorption energy, which suggests that the H₂O molecules hitting the cooled Si surface become physically adsorbed, *i.e.*, physisorbed [32].

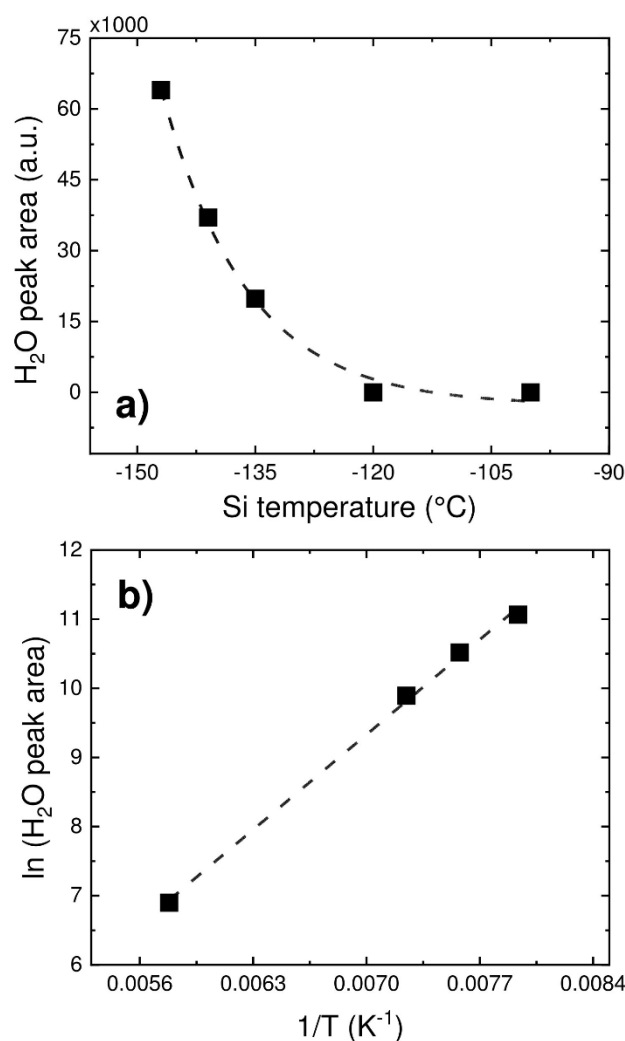


Fig. 3. a) Amount of H₂O on the analyzed surface as a function of the Si wafer temperature, under vacuum. The points were estimated from the area of the H₂O peaks identified in the O 1s XPS spectra (Fig. 2b-e) and the dashed line is an exponential fitting. b) The Arrhenius plot of the data shown in (a).

The dashed line is a linear fitting.

In physisorption, molecules from the gas or vapor phase(s) stick to the surface *via* intermolecular (van der Waals) forces, and the energy required is small, generally lower than 0.5 eV [33]. Certainly, this value depends on the extent of adsorption, as well as on both the chemical nature and the physical condition of the adsorbate and the adsorbent. For instance, Sack and Baragiola [34] found an $E = 0.45$ eV for the adsorption of water on a gold-coated

quartz microbalance, whereas the physisorption energy for various fluorine-containing molecules on Si surfaces varies between 0.13 and 0.71 eV, as reported in many studies [35–37]. Nonetheless, at such low average energies, the water molecules do not have the possibility to chemically bond to the surface, since the activation energies for chemisorption are about one order of magnitude larger [32]. The physical nature of the adsorption process discussed in the present study is also confirmed by heating up experiments. A complete recovery of the chemical state of the surface is obtained after heating up the Si wafer to the RT, which indicates that the residual water molecules desorb from the surface. As observed in both Fig. 2a and Table 1, the +25 °C (end) surface shows the same O 1s XPS spectrum aspect and almost the same oxygen relative concentration, respectively, as the surface before cooling (+25 °C sample).

Besides the concentration of the physisorbed H₂O on the analyzed surface, we also estimated the thickness d of this overlayer on Si, considering the inelastic scattering background signal for the Si 2p electrons in the ~500–100 eV BE range. The change in the background shape was discussed previously, along with Fig. 1b. By using the QUASES-Tougaard software, a buried layer model was generated, in which a continuous layer of water is expected to cover the Si surface. The IMFP for Si 2p electrons in H₂O was estimated as ~47 Å. The results obtained from the modeling are presented in Fig. 4. Although no considerable water physisorption is expected at –100 °C ($d = 0$ Å), a thickness of around 5 Å of residual H₂O molecules is estimated at –120 °C. Then, the extent of the physisorption process increases exponentially as the surface temperature decreases: at –135 °C, the H₂O multilayer thickness is ~26 Å (± 5) and at –147 °C, $d = 125$ Å (± 10). Under such a relatively thick overlayer, very few Si core photoelectrons can escape without suffering inelastic collisions (depth probed in XPS ~100 Å [25]). This will be detailed in Section 3.2.

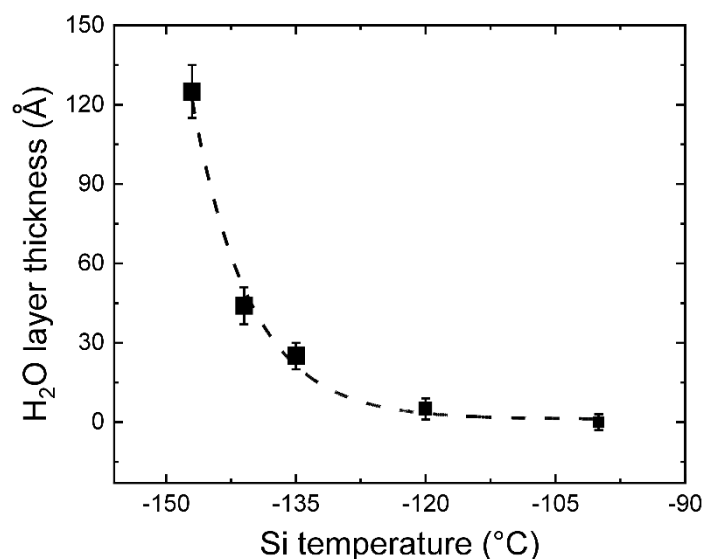


Fig. 4. The thickness of the H₂O overlayer on the analyzed surface as a function of the Si wafer temperature, under vacuum. The values were obtained using the QUASES-Generate software [22] and the TPP-2M formula [21], considering the inelastic scattering of the Si 2p photoelectrons in H₂O and a buried layer model. The dashed line is an exponential fitting.

Despite some scarce evidences previously mentioned, the present investigation has effectively addressed the issue of the residual water build-up on Si surfaces under cryogenic conditions, and established some mechanisms controlling the physical adsorption/desorption phenomena. The effects of the H₂O physisorption on semiconductors processing at $T \leq -120$ °C cannot be neglected, since the thickness of the nanolayer formed on top might be enough to shield the surface and hinder or disturb the chemical reactions involved in the etching process. These findings emphasize the role of residual water and go along with the previous studies that highlighted the SF₆ physisorption as the major barrier for semiconductors cryogenic etching at $T \leq -130$ °C.

3.2 Attenuation and energy shift of Si photoelectrons

The effects of water build-up on the Si surface are hereafter discussed in the light of the narrow Si 2p XPS core level spectra. First, one notices from Fig. 5a that the intensity of the detected peaks in the Si 2p region decreases progressively as the surface temperature is cooled

down from RT to $-141\text{ }^{\circ}\text{C}$. Moreover, at the lowest temperature, the peaks almost disappear. This behavior is in line with the quantitative data presented in Table 1, where the relative atomic concentration of Si decreases from 63% at RT to 4% at $-147\text{ }^{\circ}\text{C}$. Such a strong reduction in the amount of Si 2p photoelectrons detected is due to the water layer physisorbed over the cooled Si substrate, as discussed before. Indeed, the oxygen concentration increases as the silicon concentration decreases (Table 1).

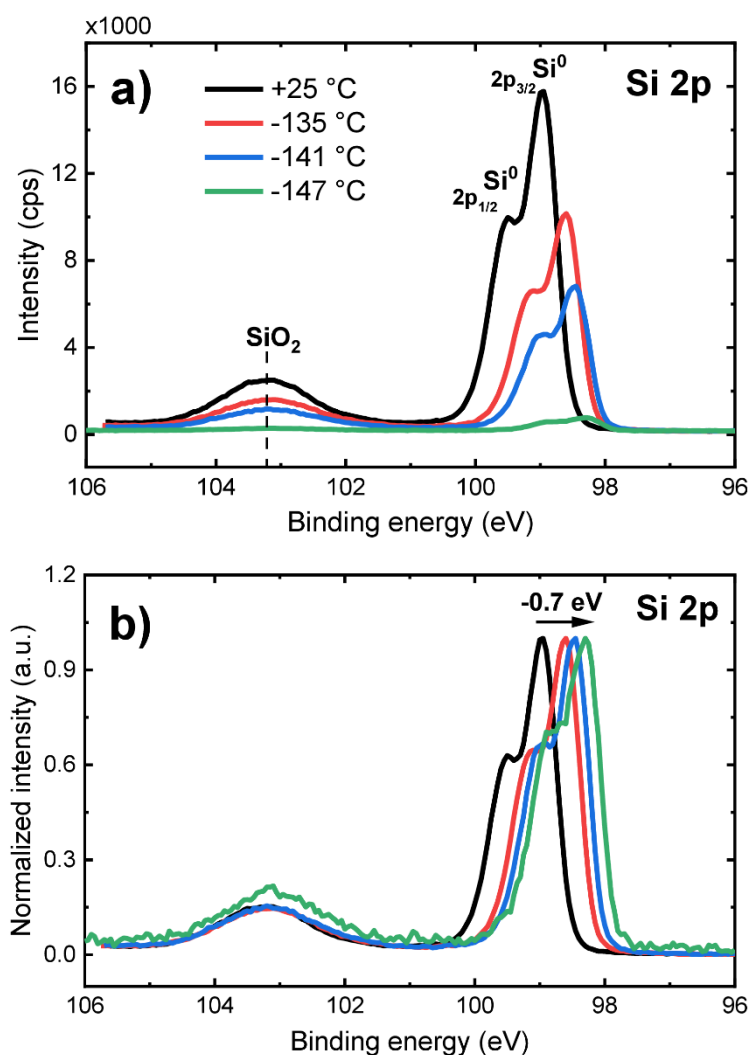


Fig. 5. a) Si 2p XPS spectra of the analyzed surface at different Si wafer temperatures, under vacuum, and b) the same spectra at normalized intensity, relative to each Si $2p_{3/2}$ peak maxima.

To establish the link between these two variables, we calculated the attenuation of the Si 2p photoelectrons due to the presence of the residual water overlayer, using the Beer-Lambert

law (described in Section 2). The calculated values are plotted in Fig. 6 (open circles) as a function of the surface temperature. They take in account the different thicknesses of the water overlayer (Fig. 4), the IMFP for Si 2p electrons in H₂O, and the intensity I_0 of the Si 2p peak obtained experimentally from the XPS spectrum of the RT sample (no water on the surface). The evolution of the calculated values in Fig. 6 reveals the exponential factor of the Beer-Lambert law, since the intensity of the photoelectrons from the Si substrate is expected to be reduced exponentially as they pass through the H₂O overlayer. For comparison purposes, the measured points, obtained experimentally from the XPS spectra of the Si surface at different temperatures, are also plotted in Fig. 6 (closed squares). One can observe that the calculated and the measured data agreed very well, confirming the attenuation phenomenon due to the presence of an overlayer of water on the Si surface. Lastly, the same procedure was applied to the C 1s photoelectrons, and the resulting graph is shown in Fig. S4 (Supplementary Material). A similar behavior is observed, which means that the adventitious carbon thin layer on the Si surface is also shielded by the residual water overlayer as the surface becomes colder.

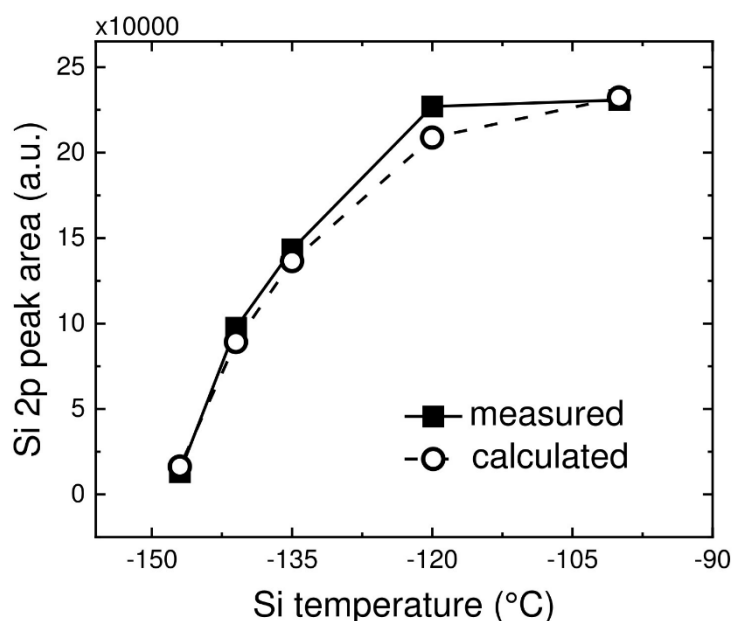


Fig. 6. Amount of Si on the analyzed surface as a function of the Si wafer temperature. The solid squares refer to the measured XPS data, from the area under the Si 2p region (Fig. 5a), whereas the open circles were calculated using the Beer-Lambert law, considering the attenuation of the Si 2p region due to the H₂O layer.

The low temperature has also an effect on the peak position of Si photoelectrons collected during the XPS analysis. Fig. 5a shows that, at RT, the Si⁰ (Si–Si bond in bulk Si) presents a spin orbit splitting with the 2p_{3/2} and 2p_{1/2} doublet centered at 99.0 and 99.6 eV, respectively. One notices also a single peak at 103.2 eV, that corresponds to the native SiO₂ layer on the non-cleaned Si surface [24,38]. As temperature decreases, the SiO₂ peak center remains at the same position. However, the Si doublet shows a progressive shift in the BE scale, toward lower values. For instance, at –147 °C, the Si 2p_{3/2} peak is centered at 98.3 eV. Thus, the binding energy shift measured experimentally is –0.7 eV from RT to –147 °C, as clearly observed in Fig. 5b, where the spectra intensities were normalized to the respective Si 2p_{3/2} peak maxima.

The shift in the binding energy could be related the temperature-dependent Fermi level, which is known to vary in extrinsic (doped) semiconductors with temperature. This is valid for the Si photoelectrons arising from the Si wafer (semiconductor) but not from the SiO₂ native layer (insulator). Briefly, in the present case, where a p-type doped silicon wafer was used, the Fermi level (E_F) is known to move closer to the valence band edge (E_v) with decreasing temperature [39,40]. Since the binding energy of a core level photoelectron is relative to the Fermi level position in XPS, at cryogenic temperatures, the BE of the Si 2p photoelectrons is expected to be slightly lower compared to the BE obtained for the surface at RT, due to the lower Fermi level position. The shift to lower energies observed experimentally in Fig. 5 seems to agree with this discussion and indicates that the doping of the Si wafer is a p-type [39], as already mentioned in Section 2. It is important to notice that

this is a qualitative discussion, and calculations/additional experiments are required to establish accurately the magnitude of the BE shift with temperature (out of scope of this study).

3.3 Surface contamination by residual fluorine compounds

So far, we have focused our discussion on the physisorption of residual water molecules on Si, at cryogenic temperatures. Although this was the dominant process identified in our XPS study, the adsorption of other residual gases could also be detected for $T \leq -100$ °C. For instance, a low-intensity N 1s XPS peak due to residual N₂ gas was noticed on the Si surface, at a BE ~402 eV. The relative N 1s concentration was always < 0.5% and, thus, not considered. A more interesting behavior was observed in the F 1s core level region, which suggests the adsorption of fluorine-based compounds on the Si surface as temperature decreases. Indeed, fluorine is known to be found on the walls of most of plasma etching reactors. Fluorine species are very reactive and can combine with other residual compounds, which usually adsorb on the surfaces undergoing a plasma-treatment. We show henceforth that this is true even without a plasma, *i.e.*, under high vacuum, if the surface temperature is sufficiently low.

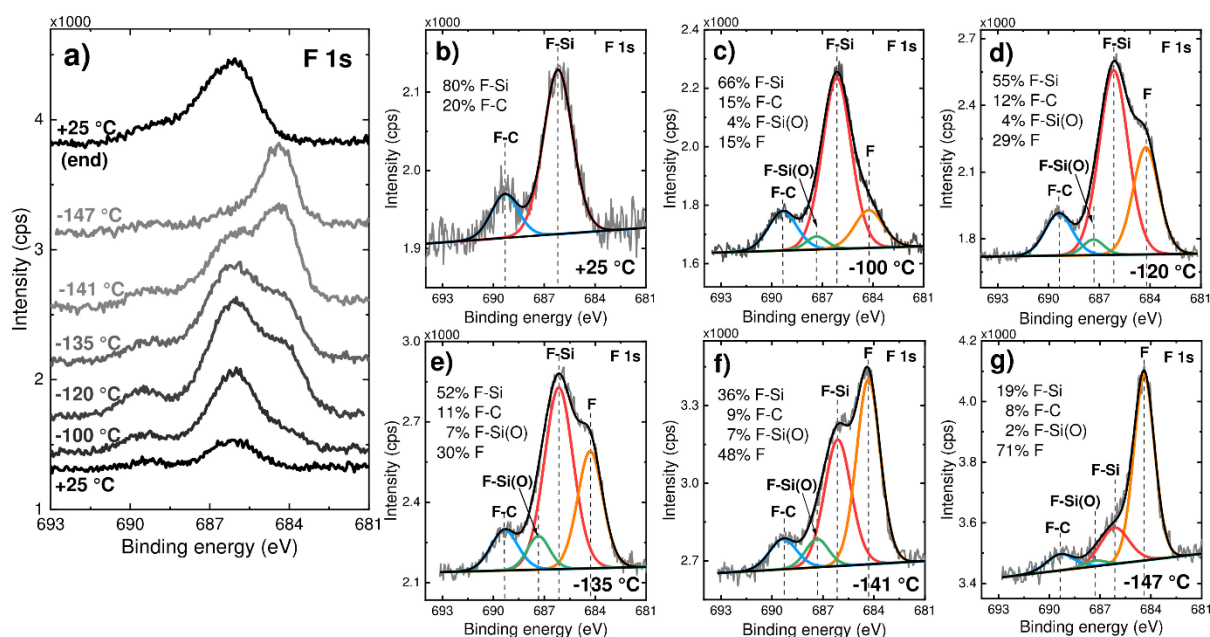


Fig. 7. a) Evolution of the F 1s XPS peak shape as a function of the Si wafer temperature, under vacuum, and b-e) the components suggested for each F 1s XPS spectrum shown in (a) along with the estimated amount of the chemical bonding/species identified in the same spectra.

Fig. 7a shows the evolution of the F 1s XPS narrow scans of the Si surface as a function of temperature. One notices considerable changes in both the fluorine peak intensity and position depending on the surface temperature. To begin, at RT and without any previous cooling, a low-intensity F 1s peak is detected by XPS, which corresponds to a relative atomic concentration <1% on the surface of the pristine Si sample (Table 1). Moreover, the peak fitting in Fig. 7b shows two main components at 686.15 and 689.35 eV, which correspond to F–Si and F–C bonds, respectively [6,24,41]. The former is due to a superficial SiF compound likely remaining from the Si wafer manufacturing process, whereas the latter is due to superficial contamination from packaging or residual CF_x compounds, as also confirmed by the respective C 1s spectrum, see Fig. S3 (Supplementary Material). When this surface is cooled down to –100 °C, the concentration of fluorine on the surface increases to 2%, due to the adsorption of residual fluorine desorbed from chamber walls. As observed in Fig. 7c, further F–Si bonds are created, and new contributions appear at 687.35 eV due to F–Si(O) bonds [6,42,43] and at 684.30 eV. The latter, at such a low binding energy, could be ascribed to adsorbed fluorine (simply indicated as “F” in the spectra), as reported elsewhere [44–46], although it could also be attributed to various metal fluorides [24]. By lowering the temperature even further, to –120 °C, all four contributions described above increase in intensity, as seen in Fig. 7d, and the F 1s concentration on the surface rises to 3%. It is worth noting that the peak at 684.30 eV doubles its intensity from –100 to –120 °C. The low temperature is clearly favoring the adsorption of various fluorine species.

As previously discussed, for $T < -120$ °C, H₂O build-up on the surface becomes important. Thus, at $T = -135$ °C, the relative F 1s concentration slightly decreases to 2%, due

to a higher relative concentration of O 1s. Besides, Fig. 7e shows that the distribution of the different chemical bonds in the F 1s spectrum remains similar as compared to the $-120\text{ }^{\circ}\text{C}$ case. Precisely, the fluorine in F–Si bonds accounts for approximately 53% of the F 1s photoelectrons detected, whereas “adsorbed F” occupies 30% of the F 1s spectrum. However, this distribution changes at $-141\text{ }^{\circ}\text{C}$ (Fig. 7f), where “adsorbed F” dominates (48% of the F 1s spectrum) over F–Si bonds (36%). Lastly, at $-147\text{ }^{\circ}\text{C}$, the intensity of the “adsorbed F” component reaches its maximum. One notices also that the relative concentration of fluorine decreases to 1% at $-147\text{ }^{\circ}\text{C}$ (Table 1). This could be related to the pronounced increase of the oxygen concentration in this sample, which indicates that the adsorption of water prevails much over the fluorine and its compounds. It could be also considered that the fluorine-adsorbed layer is shielded by the water overlayer. Nonetheless, it is difficult to determine the spatial distribution of fluorine in the analyzed surface, due to the low F 1s concentration.

To finish, the Si wafer was heated up to RT, to investigate a possible desorption of fluorine-based compounds with temperature. The XPS analysis at $+25\text{ }^{\circ}\text{C}$ (end) showed that the fluorine concentration on the surface is around 2%. This is higher compared to the concentration value obtained before all cooling procedures. Therefore, part of the fluorine adsorbed at low temperatures remains incorporated to the Si surface after warming up the sample, which suggests a chemisorption mechanism. Specifically, fluorine is chemically adsorbed in F–Si, F–Si(O), and F–C bonds, as shown in Fig. S5 (Supplementary Material). It is important to notice that the peak at 684.30 eV disappears after heating up the sample. This indicates that a physisorption mechanism is also taking place. Finally, Fig. 7a evinces clearly the changes in both the F 1s peak intensity and binding energy between the $-147\text{ }^{\circ}\text{C}$ and $+25\text{ }^{\circ}\text{C}$ (end) conditions.

3.4 Surface evolution with temperature: an overview

To summarize our findings, a schematic representation of the XPS-probed surface is proposed in Fig. 8, in a cross-section view, for selected temperatures. The pristine Si wafer (Fig. 8a) surface presents a native SiO₂ layer and a contamination layer, composed of various carbon- and fluorine-based compounds.

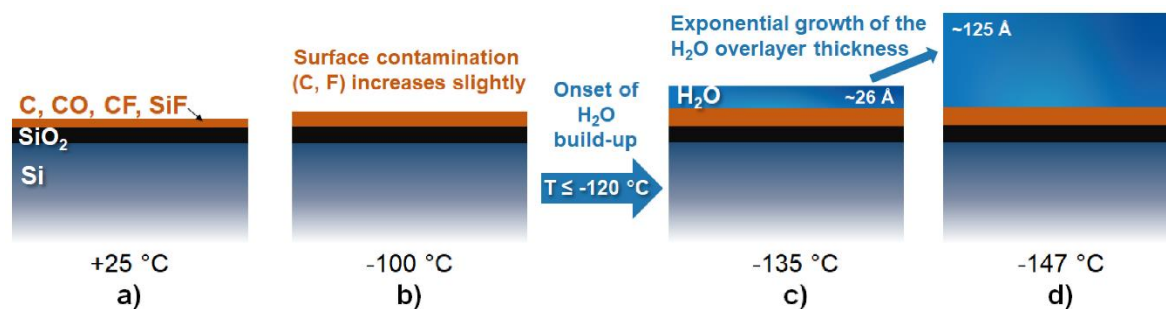


Fig. 8. Schematics of the studied Si sample surface in a cross-section view, at different temperatures.

Then, under high vacuum, the Si wafer temperature is decreased to $-100\text{ }^{\circ}\text{C}$ (Fig. 8b), which is the typical temperature used in Si cryogenic etching. The chemical state of the surface remains practically unchanged, with only a small increase in the carbon and fluorine concentrations. This is due to both the chemical and physical adsorption of carbon- and fluorine-based compounds, which naturally desorb from chamber walls as residual molecules and stick to the cooled surface. The concentration of these compounds on the surface continues to rise as temperature decreases to $-120\text{ }^{\circ}\text{C}$. At this temperature, we also establish the onset of water physical adsorption, with an overlayer thickness estimated to $\sim 5\text{ \AA}$. Residual water molecules likely stem from outgassing of reactor walls as well as from real or virtual leaks. The thickness of the H₂O overlayer increases to $\sim 26\text{ \AA}$ at $-135\text{ }^{\circ}\text{C}$ (Fig. 8c), indicating that the cooled surface retains more efficiently the residual water vapor at lower temperatures. The concentration of fluorine, carbon, and silicon decreases, since the water overlayer partially shields the Si bulk material and both the native SiO₂ and the C,F-contaminant layers. For even lower temperatures, the water build-up on the surface follows an exponential law. At $-147\text{ }^{\circ}\text{C}$ (Fig. 8d), the H₂O overlayer thickness is estimated to $\sim 125\text{ \AA}$, which is approximately the theoretical limit of depth detection in XPS analysis. Therefore, the

bulk silicon is barely probed in this case. Finally, it was possible to identify the physisorption of fluorine at $-147\text{ }^{\circ}\text{C}$, although its spatial distribution could not be determined. Therefore, it is not schematically represented in the figure. After warming the sample back to RT, the surface state is similar to that represented in Fig. 8b.

Conclusions

The present investigation has addressed the issue of residual gas adsorption on a cooled surface under high vacuum. *Quasi in situ* XPS analysis showed that water and fluorine, both of them likely stemming from leaks and outgassing of chamber walls, are the main species adsorbed to the Si surface at temperatures between -120 and $-147\text{ }^{\circ}\text{C}$. Water build-up is the dominant process, and follows an exponential, anti-Arrhenius-type behavior as surface temperature decreases, with an energy of physisorption estimated to 0.169 eV . In addition, water is completely desorbed after warming up the surface at room temperature, which confirms the physical (reversible) nature of the adsorption/desorption process. Adsorbed fluorine is also detected on the surface at low temperatures, although in a much lower concentration. Nonetheless, due to its strong reactivity, fluorine-based compounds remain on the surface after heating up the sample, suggesting a chemisorption (irreversible) process.

These findings emphasize the role of residual water on surface coverage in cryogenic conditions and complement the limited available literature on the low temperature limits for semiconductors etching. Indeed, the effects of the water physisorption on Si processing at $T \leq -120\text{ }^{\circ}\text{C}$ could not be neglected, since the thickness of the H_2O outermost nanolayer might be enough to shield the Si surface and hinder or disturb the chemical reactions involved in the etching process. Finally, this study provides an insight on the most influencing residual gases and contaminants found in a typical plasma-etching reactor, to be attentively considered before the processing of Si or other semiconductor materials at low temperatures.

Acknowledgements

Authors thank the CNRS “Réseau des Plasmas Froids” for access to the Optimist instrument.

This work was supported by the ANR project 20-CE24-0014 “PSICryo” and the CNRS program Emergence@INC2022 “OPERA”.

References

- [1] S. Aachboun, P. Ranson, Deep anisotropic etching of silicon, *Journal of Vacuum Science & Technology A*. 17 (1999) 2270–2273. <https://doi.org/10.1116/1.581759>.
- [2] M.J. de Boer, J.G.E. Gardeniers, H.V. Jansen, E. Smulders, M.-J. Gilde, G. Roelofs, J.N. Sasserath, M. Elwenspoek, Guidelines for etching silicon MEMS structures using fluorine high-density plasmas at cryogenic temperatures, *Journal of Microelectromechanical Systems*. 11 (2002) 385–401. <https://doi.org/10.1109/JMEMS.2002.800928>.
- [3] M.D. Henry, C. Welch, A. Scherer, Techniques of cryogenic reactive ion etching in silicon for fabrication of sensors, *Journal of Vacuum Science & Technology A*. 27 (2009) 1211–1216. <https://doi.org/10.1116/1.3196790>.
- [4] R. Dussart, T. Tillocher, P. Lefauchaux, M. Boufnichel, Plasma cryogenic etching of silicon: from the early days to today’s advanced technologies, *Journal of Physics D: Applied Physics*. 47 (2014) 123001. <https://doi.org/10.1088/0022-3727/47/12/123001>.
- [5] X. Mellhaoui, R. Dussart, T. Tillocher, P. Lefauchaux, P. Ranson, M. Boufnichel, L.J. Overzet, SiOxFy passivation layer in silicon cryoetching, *Journal of Applied Physics*. 98 (2005) 104901. <https://doi.org/10.1063/1.2133896>.
- [6] J. Pereira, L.E. Pichon, R. Dussart, C. Cardinaud, C.Y. Duluard, E.H. Oubensaid, P. Lefauchaux, M. Boufnichel, P. Ranson, In situ x-ray photoelectron spectroscopy analysis of SiOxFy passivation layer obtained in a SF6/O2 cryoetching process, *Appl. Phys. Lett.* 94 (2009) 071501. <https://doi.org/10.1063/1.3085957>.
- [7] T. Tillocher, R. Dussart, X. Mellhaoui, P. Lefauchaux, M. Boufnichel, P. Ranson, Silicon cryo-etching of deep holes, *Microelectronic Engineering*. 84 (2007) 1120–1123. <https://doi.org/10.1016/j.mee.2007.01.148>.
- [8] M. Boufnichel, P. Lefauchaux, S. Aachboun, R. Dussart, P. Ranson, Origin, control and elimination of undercut in silicon deep plasma etching in the cryogenic process, *Microelectronic Engineering*. 77 (2005) 327–336. <https://doi.org/10.1016/j.mee.2004.12.002>.
- [9] G Craciun, M A Blauw, E van der Drift, P M Sarro, P J French, Temperature influence on etching deep holes with SF6/O2 cryogenic plasma, *Journal of Micromechanics and Microengineering*. 12 (2002) 390. <https://doi.org/10.1088/0960-1317/12/4/307>.
- [10] G. Antoun, R. Dussart, T. Tillocher, P. Lefauchaux, C. Cardinaud, A. Girard, S. Tahara, K. Yamazaki, K. Yatsuda, J. Faguet, K. Maekawa, The role of physisorption in the cryogenic etching process of silicon, *Japanese Journal of Applied Physics*. 58 (2019) SEEB03. <https://doi.org/10.7567/1347-4065/ab1639>.
- [11] S. Tinck, T. Tillocher, V. Georgieva, R. Dussart, E. Neyts, A. Bogaerts, Concurrent effects of wafer temperature and oxygen fraction on cryogenic silicon etching with SF6/O2 plasmas, *Plasma Processes and Polymers*. 14 (2017) 1700018. <https://doi.org/10.1002/ppap.201700018>.
- [12] S. Tachi, K. Tsujimoto, S. Okudaira, Low-temperature reactive ion etching and microwave plasma etching of silicon, *Appl. Phys. Lett.* 52 (1988) 616–618. <https://doi.org/10.1063/1.99382>.

- [13] P.Y. Tessier, T. Chevolleau, C. Cardinaud, B. Grolleau, An XPS study of the SF₆ reactive ion beam etching of silicon at low temperatures, *Nuclear Instruments and Methods in Physics Research Section B: Beam Interactions with Materials and Atoms*. 155 (1999) 280–288. [https://doi.org/10.1016/S0168-583X\(99\)00451-6](https://doi.org/10.1016/S0168-583X(99)00451-6).
- [14] H. Jansen, M. de Boer, H. Wensink, B. Kloeck, M. Elwenspoek, The black silicon method. VIII. A study of the performance of etching silicon using SF₆/O₂-based chemistry with cryogenical wafer cooling and a high density ICP source, *Microelectronics Journal*. 32 (2001) 769–777. [https://doi.org/10.1016/S0026-2692\(01\)00039-8](https://doi.org/10.1016/S0026-2692(01)00039-8).
- [15] J.W. Bartha, J. Greschner, M. Puech, P. Maquin, Low temperature etching of Si in high density plasma using SF₆/O₂, *Microelectronic Engineering*. 27 (1995) 453–456. [https://doi.org/10.1016/0167-9317\(94\)00144-J](https://doi.org/10.1016/0167-9317(94)00144-J).
- [16] G. Antoun, T. Tillocher, A. Girard, P. Lefauchaux, J. Faguet, H. Kim, D. Zhang, M. Wang, K. Maekawa, C. Cardinaud, R. Dussart, Cryogenic nanoscale etching of silicon nitride selectively to silicon by alternating SiF₄/O₂ and Ar plasmas, *Journal of Vacuum Science & Technology A*. 40 (2022) 052601. <https://doi.org/10.1116/6.0001885>.
- [17] IMN, “Optimist” plasma chamber, (n.d.). <https://www.cnrs-imn.fr/index.php/themes/procedes-de-gravure/593-reacteur-plasma-optimist-2>.
- [18] N. Fairley, V. Fernandez, M. Richard-Plouet, C. Guillot-Deudon, J. Walton, E. Smith, D. Flahaut, M. Greiner, M. Biesinger, S. Tougaard, D. Morgan, J. Baltrusaitis, Systematic and collaborative approach to problem solving using X-ray photoelectron spectroscopy, *Applied Surface Science Advances*. 5 (2021) 100112. <https://doi.org/10.1016/j.apsadv.2021.100112>.
- [19] M.C. Biesinger, Accessing the robustness of adventitious carbon for charge referencing (correction) purposes in XPS analysis: Insights from a multi-user facility data review, *Applied Surface Science*. 597 (2022) 153681. <https://doi.org/10.1016/j.apsusc.2022.153681>.
- [20] S. Tanuma, C.J. Powell, D.R. Penn, Calculations of electron inelastic mean free paths. V. Data for 14 organic compounds over the 50–2000 eV range, *Surface and Interface Analysis*. 21 (1994) 165–176. <https://doi.org/10.1002/sia.740210302>.
- [21] S. Tougaard, Quantitative analysis of the inelastic background in surface electron spectroscopy, *Surface and Interface Analysis*. 11 (1988) 453–472. <https://doi.org/10.1002/sia.740110902>.
- [22] S. Tougaard, Improved XPS analysis by visual inspection of the survey spectrum, *Surface and Interface Analysis*. 50 (2018) 657–666. <https://doi.org/10.1002/sia.6456>.
- [23] M.H. Engelhard, D.R. Baer, A. Herrera-Gomez, P.M.A. Sherwood, Introductory guide to backgrounds in XPS spectra and their impact on determining peak intensities, *Journal of Vacuum Science & Technology A*. 38 (2020) 063203. <https://doi.org/10.1116/6.0000359>.
- [24] J.F. Moulder, W.F. Stickle, P.E. Sobol, K.D. Bomben, *Handbook of X-Ray Photoelectron Spectroscopy*, Physical Electronics Division, Perkin-Elmer Corp., Eden Prairie, 1992.
- [25] D. Briggs, M.P. Seah, *Practical surface analysis: Auger and X-ray photoelectron spectroscopy*, John Wiley and Sons Ltd, Chichester, 1983.
- [26] D. Goodacre, M. Blum, C. Buechner, H. Hoek, S.M. Gericke, V. Jovic, J.B. Franklin, S. Kittiwatanakul, T. Söhnel, H. Bluhm, K.E. Smith, Water adsorption on vanadium oxide thin films in ambient relative humidity, *J. Chem. Phys.* 152 (2020) 044715. <https://doi.org/10.1063/1.5138959>.
- [27] J.H. Linn, W.E. Swartz, An XPS study of the water adsorption/desorption characteristics of transition metal oxide surfaces: Microelectronic implications,

- Applications of Surface Science. 20 (1984) 154–166. [https://doi.org/10.1016/0378-5963\(84\)90335-0](https://doi.org/10.1016/0378-5963(84)90335-0).
- [28] M. Fingerle, S. Tengeler, W. Calvet, T. Mayer, W. Jaegermann, Water Interaction with Sputter-Deposited Nickel Oxide on n-Si Photoanode: Cryo Photoelectron Spectroscopy on Adsorbed Water in the Frozen Electrolyte Approach, *Journal of The Electrochemical Society*. 165 (2018) H3148. <https://doi.org/10.1149/2.0191804jes>.
- [29] C.T. Au, M.W. Roberts, An XPS study of the influence of chemisorbed oxygen on the adsorption of ethylene and water vapour by Cu (110) and Cu (111) surfaces, *J. Chim. Phys.* 78 (1981) 921–926. <https://doi.org/10.1051/jcp/1981780921>.
- [30] A. Berman, Water vapor in vacuum systems, *Vacuum*. 47 (1996) 327–332. [https://doi.org/10.1016/0042-207X\(95\)00246-4](https://doi.org/10.1016/0042-207X(95)00246-4).
- [31] V. Aquilanti, N.D. Coutinho, V.H. Carvalho-Silva, Kinetics of low-temperature transitions and a reaction rate theory from non-equilibrium distributions, *Philosophical Transactions of the Royal Society A: Mathematical, Physical and Engineering Sciences*. 375 (2017) 20160201. <https://doi.org/10.1098/rsta.2016.0201>.
- [32] S. Roy Morrison, *The Chemical Physics of Surfaces*, 1st ed., Springer, New York, NY, 1977.
- [33] T. Lill, I.L. Berry, M. Shen, J. Hoang, A. Fischer, T. Panagopoulos, J.P. Chang, V. Vahedi, Dry etching in the presence of physisorption of neutrals at lower temperatures, *Journal of Vacuum Science & Technology A*. 41 (2023) 023005. <https://doi.org/10.1116/6.0002230>.
- [34] N.J. Sack, R.A. Baragiola, Sublimation of vapor-deposited water ice below 170 K, and its dependence on growth conditions, *Phys. Rev. B*. 48 (1993) 9973–9978. <https://doi.org/10.1103/PhysRevB.48.9973>.
- [35] R. Knizikevičius, Evaluation of desorption activation energy of SiF₄ molecules, *Vacuum*. 68 (2002) 29–30. [https://doi.org/10.1016/S0042-207X\(02\)00278-6](https://doi.org/10.1016/S0042-207X(02)00278-6).
- [36] S. Tinck, E.C. Neyts, A. Bogaerts, Fluorine–Silicon Surface Reactions during Cryogenic and Near Room Temperature Etching, *J. Phys. Chem. C*. 118 (2014) 30315–30324. <https://doi.org/10.1021/jp5108872>.
- [37] T. Chowdhury, R. Hidayat, T.R. Mayangsari, J. Gu, H.-L. Kim, J. Jung, W.-J. Lee, Density functional theory study on the fluorination reactions of silicon and silicon dioxide surfaces using different fluorine-containing molecules, *Journal of Vacuum Science & Technology A*. 37 (2019) 021001. <https://doi.org/10.1116/1.5081490>.
- [38] J. Fraxedas, M. Schütte, G. Sauthier, M. Tallarida, S. Ferrer, V. Carlino, E. Pellegrin, In situ XPS analysis of the electronic structure of silicon and titanium thin films exposed to low-pressure inductively-coupled RF plasma, *Applied Surface Science*. 542 (2021) 148684. <https://doi.org/10.1016/j.apsusc.2020.148684>.
- [39] A.S. Grove, *Physics and Technology of Semiconductor Devices*, 1st ed., Wiley, 1991.
- [40] H. Mathieu, H. Fanet, *Physique des semiconducteurs et des composants électroniques*, 6th ed., Dunod, Paris, 2009.
- [41] C. Cardinaud, A. Rhounna, G. Turban, B. Grolleau, Contamination of Silicon Surfaces Exposed to CHF₃ Plasmas: An XPS Study of the Film and the Film-Surface Interface, *Journal of The Electrochemical Society*. 135 (1988) 1472. <https://doi.org/10.1149/1.2096034>.
- [42] Ch. Cardinaud, G. Turban, Mechanistic studies of the initial stages of etching of Si and SiO₂ in a CHF₃ plasma, *Applied Surface Science*. 45 (1990) 109–120. [https://doi.org/10.1016/0169-4332\(90\)90061-4](https://doi.org/10.1016/0169-4332(90)90061-4).
- [43] A. Ermolieff, F. Martin, A. Amouroux, S. Marthon, J.F.M. Westendorp, Surface composition analysis of HF vapour cleaned silicon by X-ray photoelectron spectroscopy,

Applied Surface Science. 48–49 (1991) 178–184. [https://doi.org/10.1016/0169-4332\(91\)90327-G](https://doi.org/10.1016/0169-4332(91)90327-G).

- [44] G. Nansé, E. Papirer, P. Fioux, F. Moguet, A. Tressaud, Fluorination of carbon blacks: An X-ray photoelectron spectroscopy study: I. A literature review of XPS studies of fluorinated carbons. XPS investigation of some reference compounds, *Carbon*. 35 (1997) 175–194. [https://doi.org/10.1016/S0008-6223\(96\)00095-4](https://doi.org/10.1016/S0008-6223(96)00095-4).
- [45] J.-M. Lee, S.J. Kim, J.W. Kim, P.H. Kang, Y.C. Nho, Y.-S. Lee, A high resolution XPS study of sidewall functionalized MWCNTs by fluorination, *Journal of Industrial and Engineering Chemistry*. 15 (2009) 66–71. <https://doi.org/10.1016/j.jiec.2008.08.010>.
- [46] C. Struzzi, M. Scardamaglia, A. Hemberg, L. Petaccia, J.-F. Colomer, R. Snyders, C. Bittencourt, Plasma fluorination of vertically aligned carbon nanotubes: functionalization and thermal stability, *Beilstein Journal of Nanotechnology*. 6 (2015) 2263–2271. <https://doi.org/10.3762/bjnano.6.232>.